

Characterization of the background for a neutrino search with the HAWC observatory

A. Albert,¹ R. Alfaro,² C. Alvarez,³ J.R. Angeles Camacho,² J.C. Arteaga-Velázquez,⁴
K.P. Arunbabu,⁵ E. Belmont-Moreno,² K.S. Caballero-Mora,³ T. Capistrán,⁶
A. Carramiñana,⁷ S. Casanova,⁸ U. Cotti,⁴ J. Cotzomi,⁹ S. Coutiño de León,⁷
E. De la Fuente,^{10,11} R. Diaz Hernandez,⁷ M. A. DuVernois,¹² M. Durocher,¹
C. Espinoza,² K.L. Fan,¹³ N. Fraija,⁶ D. Garcia,² J.A. García-González,¹⁴ F. Garfias,⁶
M.M. González,⁶ J.A. Goodman,¹³ D. Huang,¹⁵ F. Hueyotl-Zahuantitla,³
P. Hüntemeyer,¹⁵ A. Iriarte,⁶ A. Jardin-Blicq,^{16,17,18} D. Kieda,¹⁹ A. Lara,⁵
W.H. Lee,⁶ H. León Vargas,^{2,*} A.L. Longinotti,⁶ G. Luis-Raya,²⁰ K. Malone,¹
J. Martínez-Castro,²¹ J.A. Matthews,²² P. Miranda-Romagnoli,²³ J.A. Morales-Soto,⁴
E. Moreno,⁹ A. Nayerhoda,⁸ L. Nellen,²⁴ R. Noriega-Papaqui,²³ N. Omodei,²⁵
A. Peisker,²⁶ E.G. Pérez-Pérez,²⁰ C.D. Rho,²⁷ D. Rosa-González,⁷
A. Sandoval,² J. Serna-Franco,² R.W. Springer,¹⁹ K. Tollefson,²⁶ I. Torres,⁷
R. Torres-Escobedo,^{10,28} F. Ureña-Mena,⁷ L. Villaseñor,⁹ H. Zhou,²⁸ and C. de León⁴

(The HAWC Collaboration)

¹*Physics Division, Los Alamos National Laboratory, Los Alamos, NM, USA*

²*Instituto de Física, Universidad Nacional Autónoma de México, Ciudad de México, México*

³*Universidad Autónoma de Chiapas, Tuxtla Gutiérrez, Chiapas, México*

⁴*Universidad Michoacana de San Nicolás de Hidalgo, Morelia, Mexico*

⁵*Instituto de Geofísica, Universidad Nacional
Autónoma de México, Ciudad de Mexico, Mexico*

⁶*Instituto de Astronomía, Universidad Nacional
Autónoma de México, Ciudad de Mexico, Mexico*

⁷*Instituto Nacional de Astrofísica, Óptica y Electrónica, Puebla, Mexico*

⁸*Institute of Nuclear Physics Polish Academy of Sciences,
PL-31342 IFJ-PAN, Krakow, Poland*

⁹*Facultad de Ciencias Físico Matemáticas,
Benemérita Universidad Autónoma de Puebla, Puebla, Mexico*

¹⁰*Departamento de Física, Centro Universitario de Ciencias Exactas e Ingenierías,*

Universidad de Guadalajara, Guadalajara, Mexico

¹¹*Institute for Cosmic Ray Research,*

University of Tokyo, Kashiwa, Kashiwanoha, Japan

¹²*Department of Physics and Wisconsin IceCube Particle Astrophysics Center,
University of Wisconsin-Madison, Madison, WI, USA*

¹³*Department of Physics, University of Maryland, College Park, MD, USA*

¹⁴*Tecnologico de Monterrey, Escuela de Ingeniería y Ciencias,
Ave. Eugenio Garza Sada 2501, Monterrey, N.L., Mexico, 64849*

¹⁵*Department of Physics, Michigan Technological University, Houghton, MI, USA*

¹⁶*Max-Planck Institute for Nuclear Physics, 69117 Heidelberg, Germany*

¹⁷*Department of Physics, Faculty of Science,
Chulalongkorn University, 254 Phayathai Road,
Pathumwan, Bangkok 10330, Thailand*

¹⁸*National Astronomical Research Institute of Thailand (Public Organization),
Don Kaeo, MaeRim, Chiang Mai 50180, Thailand*

¹⁹*Department of Physics and Astronomy,
University of Utah, Salt Lake City, UT, USA*

²⁰*Universidad Politecnica de Pachuca, Pachuca, Hgo, Mexico*

²¹*Centro de Investigación en Computación,
Instituto Politécnico Nacional, México City, México.*

²²*Dept of Physics and Astronomy, University of New Mexico, Albuquerque, NM, USA*

²³*Universidad Autónoma del Estado de Hidalgo, Pachuca, Mexico*

²⁴*Instituto de Ciencias Nucleares, Universidad Nacional
Autónoma de Mexico, Ciudad de Mexico, Mexico*

²⁵*Department of Physics, Stanford University: Stanford, CA 94305-4060, USA*

²⁶*Department of Physics and Astronomy,
Michigan State University, East Lansing, MI, USA*

²⁷*University of Seoul, Seoul, Rep. of Korea*

²⁸*Tsung-Dao Lee Institute & School of Physics and Astronomy,
Shanghai Jiao Tong University, Shanghai, People's Republic of China*

(Dated: March 3, 2022)

Abstract

The close location of the HAWC observatory to the largest volcano in Mexico allows to perform a search for neutrino-induced horizontal muons. The section of the volcano located at the horizon reaches values of slant depth larger than 8 km of rock, making it an excellent shield for the cosmic ray horizontal background. We report the search method and background suppression technique developed for HAWC, as well as a model that describes the remaining background produced by scattered muons. We show that by increasing the detection energy threshold we could use HAWC to search for Earth-skimming neutrinos.

I. INTRODUCTION

Neutrinos are perhaps the most elusive particles of the Standard Model. They are probes that allow us to study weak interactions and the internal structure of nucleons and nuclei [1]. At TeV energies, neutrinos allow us to test fundamental physics at energies that are not reachable at laboratories [2] and those in the ultra high energy regime (UHE), starting at ~ 100 TeV [3], point back to the most energetic particle accelerators in the Universe. In the GeV-TeV energy range neutrinos are predominantly of atmospheric origin.

Neutrino detection is a challenging task that requires special experimental conditions that range from building underground detectors, in order to avoid contamination from cosmic radiation, to requiring very large volumes of sensitive material such as ice or water to increase the probability of observing the visible signals from their weak interactions with matter. An example of such a detector is IceCube, with a 1 km^3 detection volume, that proved the existence of UHE astrophysical neutrinos [4].

Two decades ago an alternative method, called Earth-skimming, was proposed to perform neutrino detection with above ground detectors [5, 6]. It consists of using mountains, or chords through the Earth, as a target to produce charged current neutrino-nucleon interactions. A number of early above ground neutrino detectors are discussed in [7], but none have been built.

Several air shower detectors have been used to search for astrophysical neutrinos. For instance Ashra [8, 9], MAGIC [10, 11] and the Pierre Auger observatory [12, 13] have set

* hleonvar@fisica.unam.mx

upper limits on the neutrino flux at the UHE regime. Underground experiments have also searched for neutrinos associated to astrophysical sources, as for instance the detector of Crouch et al. [14] Soudan 2 [15], MACRO [16], Fréjus [17], Kolar Gold Fields [18] and LVD [19]. HAWC presented preliminary results of a neutrino search in [20, 21]. In this work we present a method to search for neutrino-induced muons with a surface air shower array, providing evidence that it is feasible to use this type of detector to search for Earth-skimming neutrinos.

II. THE HAWC OBSERVATORY

The High-Altitude Water Cherenkov (HAWC) observatory [22] is located at approximately 4100 m a.s.l. on the slopes of the Sierra Negra volcano in the state of Puebla, Mexico. The main array of HAWC consists of 300 Water Cherenkov Detectors (WCDs) distributed over a surface of 22,000 m². Each WCD is a cylindrical steel structure with a diameter of 7.3 m and 5 m tall. Inside of each of these structures is a plastic bladder that contains a water volume of approximately 200 000 litres. Each WCD is instrumented with four photomultiplier tubes (PMTs) fixed at its base.

The PMTs detect the Cherenkov light produced by charged particles as they pass through the water volume. Their calibration is performed using a laser system that sends pulses of different intensities in order to characterize the PMT response and to correct for the dependence of the timing with the light intensity, achieving nanosecond precision [23]. The timing calibration is improved to fractions of nanosecond by iterative fits to hadronic air showers [22]. All PMT pulses are digitized with the Time over Threshold (ToT) method with a double threshold with amplitudes of 1/4 and 4 photoelectrons (PEs). The signals are time stamped to 100 ps and readout by a computer farm that continuously time orders the hits of the full HAWC array and generates an event trigger if there are at least 28 PMT hits within a sliding time window of 150 ns. The events are stored including all hits 0.5 μ s before and 1 μ s after the trigger for offline analysis [24].

The main objective of HAWC is to characterize gamma-ray sources in the energy range between a few hundred GeV up a few hundred TeV. In this work we use the Pico de Orizaba volcano as both target for neutrino-nucleon interactions and as absorber for the horizontal atmospheric muon flux. Figure 1 shows the topography of the volcano obtained with

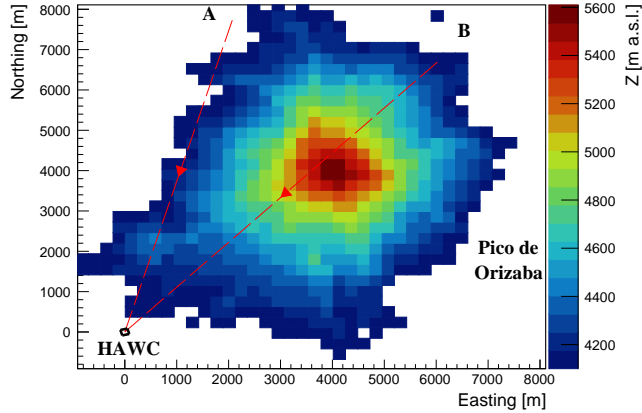


FIG. 1. Elevation map of the Pico de Orizaba volcano. The observatory footprint is shown with a black square around the origin of the coordinate system. The color code indicates the altitude above sea level. Note that HAWC is located at ≈ 4100 m a.s.l. The arrows A and B show the approximate angular region used in the analysis.

data from the Mexican National Institute of Statistics, Geography and Informatics (INEGI) [25]. The location and approximate size of the HAWC observatory is shown by the area surrounded by black lines at the origin of the coordinate system. The arrows enclose the approximate angular region used in the analysis as described below.

The method used for the neutrino search with HAWC is based on measuring the passage of the charged lepton (in the case of muons) produced in a charged current neutrino-nucleon interaction, or its highly collimated decay products (in the case of taus) [26]. This method is possible due to the modular design of the observatory that allows to use each WCD as a *pixel* and HAWC as a particle tracker.

Figure 2 shows the simulated detector response to an almost horizontal 10 TeV muon. The simulations presented on this work were prepared using the GEANT4 [27] based framework of HAWC. In Figure 2 each WCD is represented by a circle that encloses four smaller circles that depict the PMTs located inside. The time coordinate is shown with a color scale and the size of each filled circle is proportional to the magnitude of the measured charge. To ease the visualization this particular simulation does not include the noise primarily caused by vertical muons in data. However, one can notice WCDs with signals that are not contained in a straight line of WCDs. These additional hits are caused by secondary particles produced during the muon propagation, as predicted by the simulations. The time needed for the

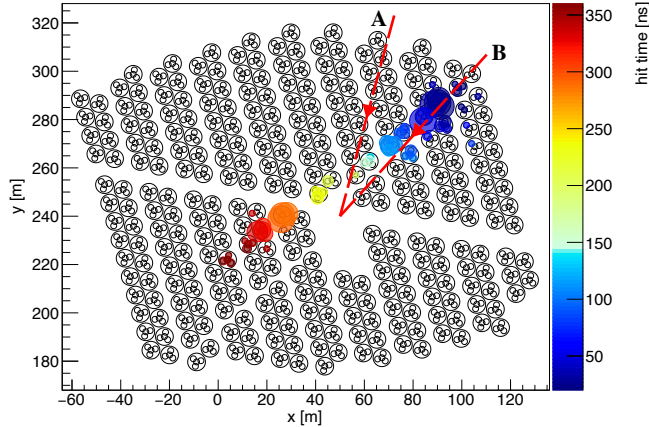


FIG. 2. Simulation of an horizontal muon passing through HAWC. The color code indicates the PMT hit time while the size of the filled circles is proportional to the measured charge. The muon track points to the thickest region of the Pico de Orizaba volcano. The arrows show the approximate angular region used in the analysis and correspond to those shown in Figure 1. The x and y axis are oriented along the Easting and Northing directions respectively.

simulated muon to propagate through the detector with this trajectory is ~ 400 ns. Due to the excellent time resolution of the instrument we can infer the propagation direction even between pairs of WCDs and verify that the particle propagates at light velocity.

The standard HAWC multiplicity trigger is general enough to capture the signals of interest for this study. However, it is reasonable to look for tracks in events where only a fraction of the total number of available PMTs are hit, in order to avoid the contamination of a muon track with secondary particles from a gamma-ray or a cosmic-ray induced air shower. This analysis is restricted to triggered events that contain at most 100 (out of a maximum of ≈ 1200) PMT hits in a $1.5 \mu\text{s}$ time window.

The data selection was based on a proxy for the detector stability: the number of consecutive subruns associated to each run. The HAWC data are archived in runs that have a maximum duration of 24 hours. Each run is subdivided in ~ 2 minute subruns, giving a maximum of 692 subruns per run. For this analysis we selected runs with at least 400 consecutive subruns. We studied data acquired during the months of June to October, 2017 and from January to May, 2018. The data selection requirement reduced the live time to approximately six months.

The processing of the data begins with the standard HAWC reconstruction algorithms

that use the charge and time of the PMT hits to determine the event energy and direction. Our tracking algorithm, described in the next section, is then run over all the PMT hits in the events.

III. TRACKING ALGORITHM

For each triggered event, the PMT hits are time ordered. We use a look up table to find if a given PMT hit is followed temporally by another signal in a different PMT in the spatial vicinity of the first signal, activated within a time window constrained by speed of light propagation. Based on full Monte Carlo (MC) simulations we optimized the time window width, allowing a 40 ns uncertainty due to the different paths light can take inside the WCDs to reach the PMTs. The search process continues until no further hits are found that follow a sequence of neighbouring WCDs.

We use a charge threshold of 4 PEs in the PMT signal in order to minimize noise contamination. This reduces the single PMT rates by a factor of ~ 4 . A minimum of two PMT hits with charge above the threshold are required in order to consider a WCD as an active *pixel* for track reconstruction. A track candidate is saved for further processing if it comprises at least nine PMT hits, setting the minimum length of a track to three *pixels*. A more strict verification of speed of light propagation is performed to the track candidate, as well as a verification that the positions of the *pixels* involved in the track can be fit using a linear function (for the muon energies that we detect the effect of the Lorentz force is negligible [28]); if this step is successful the track properties are calculated.

The angular properties of the track are calculated using the survey measurements of each WCD in the local coordinate system. The azimuth angle ϕ is calculated in the x - y plane, by fitting a straight line that passes through the centres of the first and last *pixel* involved in the track. A cut is made to the reconstructed trajectory requiring it to intersect at least 75% of the *pixels* that were identified as part of the track in the previous step. The intersection of the track with each *pixel* in the x - y plane should be of at least 4 m. We follow the convention of measuring ϕ starting from East and in clockwise direction. The elevation angle θ is obtained by combining the height and x - y positions of the WCDs that participate in the track. HAWC is located on a flat surface that limits the elevation angles that are possible to study. At present we are not able to distinguish if a muon is propagating

upwards or downwards within the array. Both trajectories share the property of having a larger amount of Cherenkov light detected at the central *pixels* of the track compared to that measured at the edges of the track. A similar direction ambiguity was also observed by dedicated neutrino detectors such as LVD [29] and Soudan 2 [15].

The final step in the processing of the track candidates consists in making very strict requirements on their isolation. This is done due to the presence of a huge background from very inclined showers that are capable of satisfying the previously mentioned set of cuts. The values of the following cuts were defined by both scanning a large number of track candidates in data and with the use of full MC simulations of muons embedded into real data noise. We defined two variables that globally characterize the event compared with the track candidate contained on it:

- Hit Activity (H_A): given by the ratio of the total number of WCDs with at least one PMT hit (without considering any charge threshold) in the $1.5 \mu\text{s}$ event window (N_{WCDs}) and the track length within the detector volume, quantified by the number of *pixels* that are associated to a track ($N_{\text{Pix}}^{\text{Track}}$), i.e.

$$H_A = N_{\text{WCDs}}/N_{\text{Pix}}^{\text{Track}}, \quad (1)$$

we cut on $H_A < 5.65$ to remove air showers. By making a ratio we allow that triggered events with long tracks to contain more PMT hits that fall outside a straight line, as shown in Figure 2, compared to shorter tracks. This cut reduces the number of track candidates by 99.83%.

- Pixel Activity (P_A): given by the ratio of the total number of *pixels* ($N_{\text{Pix}}^{\text{Tot}}$) in the event and the track length quantified by the number of *pixels* associated to the track, i.e.

$$P_A = N_{\text{Pix}}^{\text{Tot}}/N_{\text{Pix}}^{\text{Track}}, \quad (2)$$

the cut was set as $P_A < 1.5$. We expect that an horizontal muon will produce the largest fraction of PMT hits above the 4 PE threshold. However, we have to consider that there could be vertical muons in the same event that could also produce PMT hits that satisfy the charge threshold cut and thus activate additional *pixels*. This is the reason why we allow up to $\approx 50\%$ more *pixels* in the events. This cut reduces the number of track candidates by 96.13%.

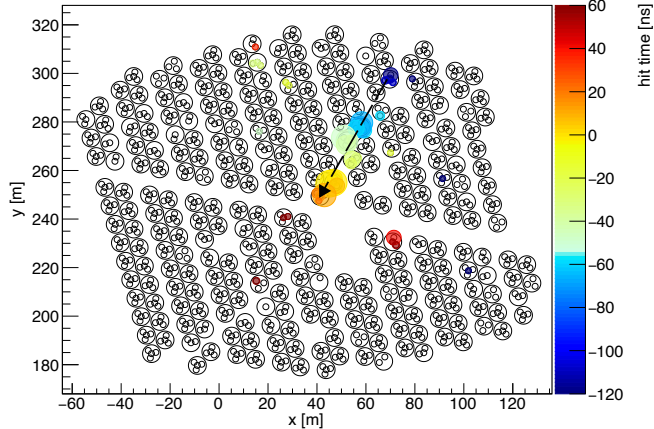


FIG. 3. Near horizontal track found in the data whose direction points to the volcano. The color code indicates the time while the size of the filled circles is proportional to the charge.

The combination of both cuts reduces the track candidate sample by 99.93%. Another possible source of contamination is artificial tracks created by combinatorial background. In order to assess its possible contribution we used a data based method. For the whole data sample we randomized the PMT locations, keeping the corresponding charge and time information. Then we ran our tracking algorithm over this randomized data set. The algorithm was able to identify artificial tracks with an average number of 0.01% of that from real track candidates, but over the whole six month live time the maximum length of these artificial tracks was of three *pixels*. We decided to make an additional cut that required tracks to have a length equal or longer than four *pixels* to completely get rid of the combinatorial background. Figure 3 shows an example of a track found in the data that points back to the Pico de Orizaba volcano.

The performance of the tracking algorithm was tested using simulated muons in the energy range [100 GeV, 5 TeV], embedded into real noise obtained from untriggered data. The detector efficiency has a strong dependence on the track azimuth angle due to the irregular distribution of WCDs in the observatory. The regions between columns and rows of WCDs produce preferential directions where both the angular resolution degrades and the rate of artificial tracks due to near horizontal air showers is increased. There are, however, several regions of the acceptance pointing to the volcano where the angular resolution is reasonably good ($< 2^\circ$).

For this analysis we restrict our search of tracks to those that point back to the base of

the Pico de Orizaba volcano, the region that provides the best shielding against atmospheric muons. We segmented the acceptance in rectangular bins of six degrees in azimuth and two degrees in elevation. By restricting our study to near horizontal tracks the measurements are less affected by reconstruction inefficiencies. We use for the analysis the six bins that have the best tracking efficiency and angular resolution ($[282^\circ, 318^\circ]$ in azimuth, delimited by the red lines in Figure 4). The angular resolution in the azimuth direction in this region is $< 2^\circ$ with the exception of the interval $[294^\circ, 300^\circ]$, where the angular resolution is $\approx 2.5^\circ$. This particular azimuth bin is however well contained by the full analysis region. The angular resolution in the elevation direction, for a reconstructed elevation $\theta_{Rec} < 2^\circ$, is of 0.7° . The angular resolution, as expected, degrades for increasing reconstructed elevation angles. For instance, for $4^\circ < \theta_{Rec} < 6^\circ$, the angular resolution is of 3.5° .

The results discussed in the next section are presented for the combination of the six bins, and also for the subregions I and II delimited by dashed lines in Figure 4.

IV. MODEL OF THE BACKGROUND FROM SCATTERED MUONS

Once we are able to reject both the background from air showers and the combinatorial one, the largest remaining background for a neutrino search with a surface array is produced by muons that are scattered towards horizontal directions and seem to point back to the volcano [30–32].

The volcano acts as a shield against the atmospheric muon flux. Therefore we need to study the effect that it produces on the muons that could be scattered. The shadow of the mountain is shown in Figure 4, that displays the values of the *line of sight mass* (LOSM) that an atmospheric muon would need to travel before reaching HAWC. The color code shows values larger than 1 kilometre water equivalent (km.w.e.). The conversion from the rock overburden measured geometrically in km to km.w.e. was done considering the composition of the volcano. This large volcanic structure was built by different processes over a time span that comprises several thousands of years, producing eruptive products of different composition, which makes it difficult to determine a single and precise value for the density of the bulk of the Pico de Orizaba. However, for the purpose of this paper, we can use mean values of andesitic rocks to approximate the density of Pico de Orizaba with a value of 2.6 g/cm^3 [33]. A study of the effects of the chemical composition on the attenuation of the

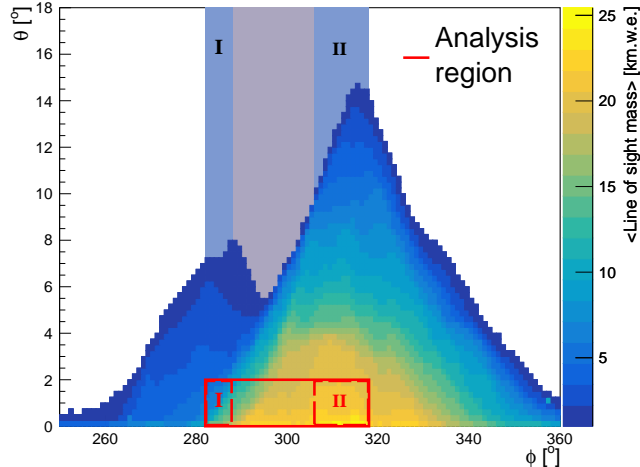


FIG. 4. Pico de Orizaba profile as seen from the center of the HAWC main array. The shaded areas behind the mountain show the solid angles where muons propagate before being scattered towards almost horizontal directions into the three analysis regions, delimited by red lines (full region and regions I and II).

muon flux can be found in [34], particularly useful in the context of muon tomography as in the recent results with the Khufu Pyramid [35].

We model the background of muons that scatter towards almost horizontal directions using geometrical arguments. The shaded areas in Figure 4 show the region above the volcano from where muons can travel unabsorbed towards HAWC and be scattered into the horizontal acceptance of the detector, faking their direction as coming from the analysis region. The darker shadings indicate the parts of the sky where muons can scatter into the analysis sub-regions I and II.

The atmospheric muon differential intensity as a function of the zenith angle close to the horizon was obtained by fitting the data available from [36] at 3200 m a.s.l., which are the closest measurements to the HAWC altitude. In Figure 5, a sample of these data shows the differential intensity as a function of the muon energy at a fixed elevation angle of $\theta=15^\circ$. For muon energies that were not available in the data set from [36] we used the results from the model presented in [37]. Since the scattering probability is inversely proportional to the muon momentum [30, 32], this background has a strong dependence on the muon energy. The scattering probability as a function of the muon energy and elevation angle was evaluated using the GEANT4 based simulation of the HAWC observatory. We calculated

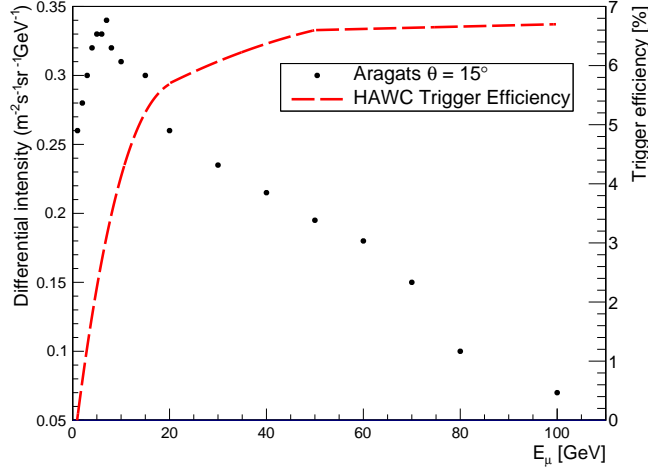


FIG. 5. Differential intensity of muons from an elevation angle of $\theta=15^\circ$, shown as black dots, from the compilation from Aragats [36]. The HAWC trigger efficiency is shown as a red line with the right hand side scale.

this probability by simulating an isotropic distribution of muons directed towards the HAWC observatory. This type of simulation is appropriate since the elevation dependence of the muon flux is taken into account by the fits to the Aragats [36] measurements. An example distribution of the scattering probability is shown in Figure 6, for 5 GeV muons. The solid line shows the fit to the simulation results used in the scattering calculation. The scatterings are almost completely dominated by muons that are deflected just enough to produce an almost horizontal trajectory, which based in our analysis strategy corresponds to trajectories that intersect at least four WCDs.

The flux of muons that are scattered towards horizontal trajectories, for any 1° bin in azimuth, is calculated using Equation 3

$$F_{Scatt}^\phi(E) = \frac{\pi}{180} \int_{\theta_i}^{\theta_f} I(E, \theta) P_{Scatt}(E, \theta) \sin \theta d\theta, \quad (3)$$

where $I(E, \theta)$ is the function that describes the muon differential intensity at energy E close to the horizon and $P_{Scatt}(E, \theta)$ is the function that describes the scattering probability at energy E and elevation angle θ obtained from the fit to simulations as in Figure 6. The integration limits in the elevation angle are given by the geometrical constrains of the mountain profile for each particular azimuth bin, i.e. we evaluate the integral starting from the highest elevation covered by the mountain profile and integrate up to $\theta_f = 18^\circ$. We simplify the azimuth dependence of the scatterings by assuming that for any particular

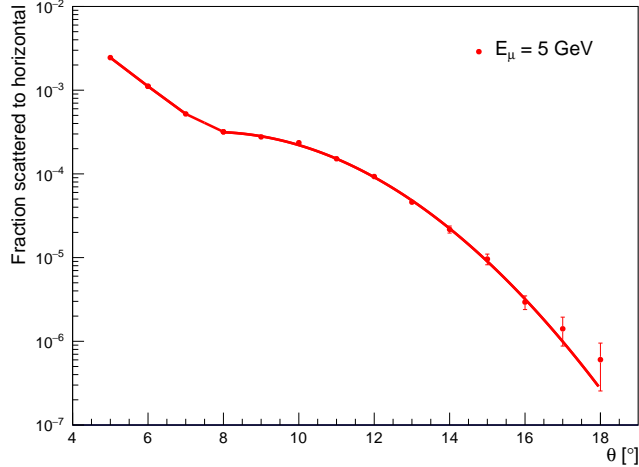


FIG. 6. Fraction of simulated 5 GeV muons that are scattered towards almost horizontal directions as a function of the elevation angle. The solid line shows the fit used in the calculations.

azimuth bin the probability that a muon can scatter in the azimuth direction and migrate to a neighbour bin cancels out due to the opposite effect happening, with the same probability, in the neighbour bin. This is of course a simplification given that the volcano is not perfectly symmetric, but given the current uncertainties in our measurements it is reasonable to use this simplification in our calculations.

We then add the contributions of the 1° bins in azimuth that go into each analysis region at a fixed energy E with Equation 4

$$F_{Scatt}(E) = \sum_{\phi} F_{Scatt}^{\phi}(E), \quad (4)$$

and finally add the contribution from muons starting at 2 GeV (the approximate detection threshold with HAWC) up to 100 GeV. We divide the result by the corresponding solid angle covered by each analysis region, as shown in Equation 5, to obtain the scattered intensity

$$I(i) = \sum_{E=2,3,\dots}^{E=100 \text{ GeV}} F_{Scatt}(E)/\Omega_i, \quad (5)$$

on the other hand the intensity from data is calculated using Equation 6

$$I(i) = \frac{N_i^{\text{Raw}}}{\Delta T(A\Omega)_i}, \quad (6)$$

where N_i^{Raw} is the raw number of tracks of the i -th bin, ΔT is the live time and $(A\Omega)_i$ is the product of the area and solid angle. The solid angle Ω_i corresponds to that covered by each

TABLE I. Mean values of the *line of sight mass* (LOSM) and effective area in the directions of interest shown in Figure 4. The column -tracks- indicates the raw number of signals detected in each region of the acceptance.

Bin	$\langle \text{LOSM} \rangle$ [km.w.e.]	$A\Omega$ [m ² sr]	Tracks
Full	$17.70^{+3.35}_{-9.23}$	$5.1 \times 10^{-2} \pm 4.7 \times 10^{-4}$	122
I	$9.54^{+1.95}_{-1.92}$	$4.1 \times 10^{-3} \pm 1.4 \times 10^{-4}$	21
II	$20.97^{+0.09}_{-0.13}$	$3.0 \times 10^{-2} \pm 3.6 \times 10^{-4}$	26

analysis region. The effective area A_i for each analysis region was obtained with Equation 7

$$A_i = \frac{N_{\text{trigg}}}{N_{\text{gen}}} \times A_{\text{gen}}, \quad (7)$$

where N_{trigg} is the number of MC tracks that trigger HAWC, N_{gen} is the number of generated tracks that point towards the observatory and whose trajectories intersect at least four WCDs, and A_{gen} is the area over which the MC muons are generated. We use MC simulations of muons embedded into real data noise. The HAWC simulations include a detailed implementation of the PMT-to-PMT relative variations in efficiency. Figure 5 shows with a red line the trigger efficiency as a function of the muon energy. The detection efficiency increases with increasing muon energy due to the larger production of secondary particles. The additional PMT hits produced by the radiative energy loss of muons allows to increase the probability to reach the multiplicity trigger requirement. At 10 TeV the trigger efficiency is $> 18\%$.

The numerical values of the product $(A\Omega)_i$ for the three analysis regions shown in Figure 4 are reported in Table I. These values correspond to the effective area of HAWC to detect muons with energies larger than 2 GeV with the analysis strategy described on this paper. The uncertainty in the effective area comes from the statistics available in the MC. Table I also shows the average LOSM values for the three selected analysis regions and the raw number of track candidates found on each analysis region. The uncertainty in the LOSM reported on Table I correspond to the maximum variation found in the distributions of values for each analysis region. The variation include the effect of changing the reference observation position throughout the HAWC platform.

Figure 7 shows the comparison of the measurement of HAWC with the result of the

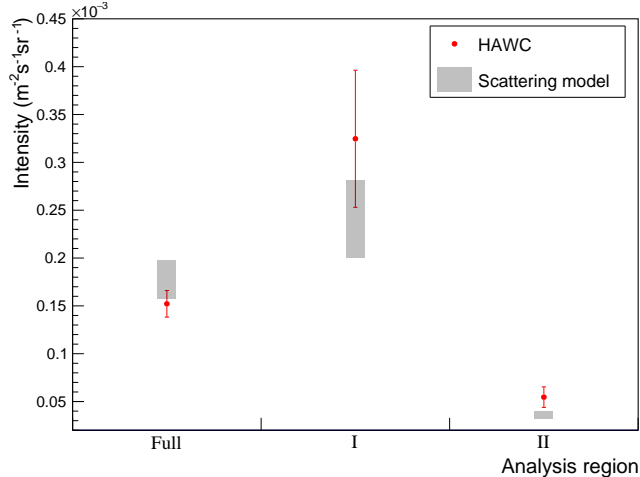


FIG. 7. Muon intensity for the analysis bins that point back to the base of the Pico de Orizaba volcano. The shaded area shows the estimation of the scattered intensity in the corresponding regions.

scattering model. There is fair agreement between the HAWC measured intensity and the scattering model. A more sophisticated estimation of the background for a neutrino search would include the propagation of muons through regions with low values (< 1 km.w.e.) of the LOSM. However, such study is beyond the scope of this paper and we consider our simple modelling sufficient for our purposes. As an uncertainty of our model we show in Figure 7 how the expected scattered intensity changes by increasing the threshold value of the LOSM used to define the mountain profile from 1 to 2 km.w.e., the allowed range is shown with the shaded area.

Given the fair agreement between our scattering model and the measurement, we can use the model to define a strategy to search for neutrino-induced muons. Figure 8 shows the predicted differential intensity of scattered muons as a function of the muon energy for the full analysis region. The solid horizontal line at the top of the figure shows the predicted integral intensity above the HAWC detection threshold which is consistent with our measurement from the full analysis region as shown in Figure 7. The dotted and dashed horizontal lines show the predicted integral intensity obtained when increasing the detection energy threshold to 60 GeV and to 80 GeV in our model. The blue shaded area shows, as a reference, the integral value of the neutrino-induced horizontal muon intensity measured by the LVD collaboration [29]. This analysis shows that by cutting in the muon energy the scattering

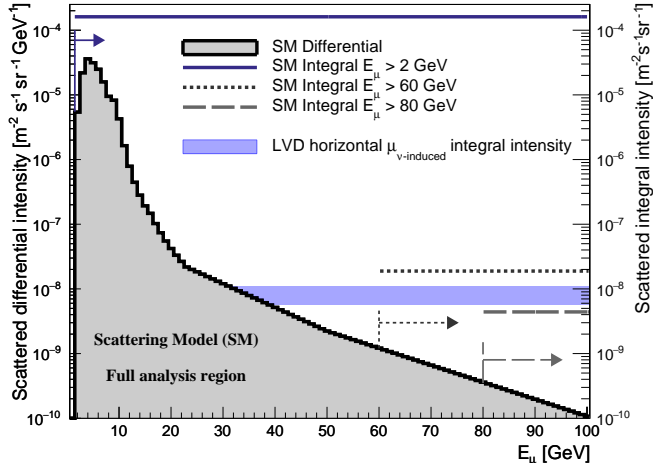


FIG. 8. Simulated energy distribution of the scattered muons that point back to the full analysis region at the base of the Pico de Orizaba volcano. The horizontal lines show the integrated intensity for different muon energy thresholds according to our model. The arrows indicate the direction of the integration over the differential intensity distribution. The integral intensity of horizontal neutrino-induced muons measured by LVD [29] is shown as reference with a blue area.

background can be reduced. For high energy muons (> 100 GeV) the background is below the intensity of neutrino-induced muons in rock as measured by the LVD experiment, opening the possibility of their detection by the HAWC observatory using the Pico de Orizaba volcano as a neutrino target and atmospheric muon filter.

The energy estimation of near horizontal muons with HAWC is not a trivial task because we are only able to sample the energy deposited by a muon. We are exploring the possibility of using the independent charge measurement from different *pixels*. The charge deposited in each *pixel* by the same muon shows fluctuations that depend on two factors: the proximity and incidence angle of the track with respect to the PMTs and fluctuations due to radiative energy losses [38, 39]. We plan to use the fact that high energy muons suffer stochastic energy losses that cause variations in the deposited charge in different *pixels* along the muon trajectory. The dynamic range of the PMTs in HAWC goes from a fraction of a PE up to thousands of PEs, and an average atmospheric muon produces ≈ 30 PEs [40], leaving ample room to characterize large energy losses. Dedicated neutrino observatories such as IceCube have made use of catastrophic energy losses to identify very high energy muons [41]. In [20] we presented preliminary results of muon signals that produce very large deposits of charge

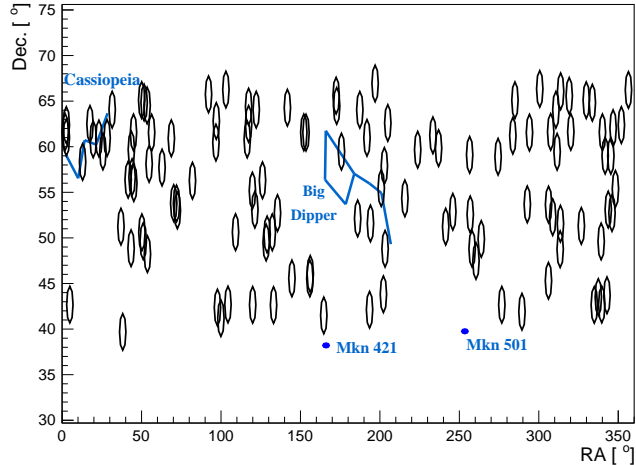


FIG. 9. Celestial coordinates for the 122 track events found in the data. The size of the circles show the average angular resolution of the tracker. The muon signals reported on this work are dominated by those of scattered atmospheric muons, the figure illustrates the field of view accessible with our analysis. The location of the Cassiopeia and Big Dipper constellations are shown as reference, as well as the Mkn 421 and Mkn 501 AGNs.

in the detector. At this moment we are not yet able to provide reliable estimations of the muon energies and will leave such results as the subject of future publications.

To further motivate the capabilities of our detection method, Figure 9 shows the projection of the reconstructed muon trajectories in celestial coordinates. The background of Figure 9 shows as reference the Cassiopeia and Big Dipper constellations, as well as the active galaxies Mkn 421 and Mkn 501. Although our detected signals are dominated by scattered muons, the figure is used to illustrate the field of view that could be used in the future once we are able to efficiently separate the high energy signals in our data.

V. CONCLUSIONS

We report on the development of a tracking strategy to reconstruct horizontal muon trajectories with the HAWC array of 300 water Cherenkov detectors, in an effort to detect Earth-skimming neutrino-induced muons from the direction of the nearby Pico de Orizaba volcano. A detailed background study was performed which indicated that scattering of low energy muons into the horizontal acceptance of the detector overwhelms the signal, but that this background can be suppressed by cutting at muon energies above ~ 100 GeV. A method

to determine the energy of the detected muons is being developed.

ACKNOWLEDGMENTS

We acknowledge the support from: the US National Science Foundation (NSF); the US Department of Energy Office of High-Energy Physics; the Laboratory Directed Research and Development (LDRD) program of Los Alamos National Laboratory; Consejo Nacional de Ciencia y Tecnología (CONACyT), México, grants 271051, 232656, 260378, 179588, 254964, 258865, 243290, 132197, A1-S-46288, A1-S-22784, cátedras 873, 1563, 341, 323, Red HAWC, México; DGAPA-UNAM grants IG101320, IN111315, IN111716-3, IN111419, IA102019, IN110621; VIEP-BUAP; PIFI 2012, 2013, PROFOCIE 2014, 2015; the University of Wisconsin Alumni Research Foundation; the Institute of Geophysics, Planetary Physics, and Signatures at Los Alamos National Laboratory; Polish Science Centre grant, DEC-2017/27/B/ST9/02272; Coordinación de la Investigación Científica de la Universidad Michoacana; Royal Society - Newton Advanced Fellowship 180385; Generalitat Valenciana, grant CIDEGENT/2018/034; Chulalongkorn University's CUniverse (CUAASC) grant; Coordinación General Académica e Innovación (CGAI-UdeG), PRODEP-SEP UDG-CA-499. Thanks to Scott Delay, Luciano Díaz and Eduardo Murrieta for technical support.

-
- [1] A. de Gouvêa, Neutrino Mass Models, *Annual Review of Nuclear and Particle Science* **66**, 197 (2016), <https://doi.org/10.1146/annurev-nucl-102115-044600>.
 - [2] M. Ackermann *et al.*, Fundamental Physics with High-Energy Cosmic Neutrinos, *Bull. Am. Astron. Soc.* **51**, 215 (2019), arXiv:1903.04333 [astro-ph.HE].
 - [3] F. Halzen, High-energy neutrino astrophysics, *Nature Physics* **13**, 232 (2017).
 - [4] M. G. Aartsen *et al.* (IceCube Collaboration), Evidence for High-Energy Extraterrestrial Neutrinos at the IceCube Detector, *Science* **342**, 1242856–1242856 (2013).
 - [5] D. Fargion, A. Aiello, and R. Conversano, Horizontal tau air showers from mountains in deep valley: Traces of UHECR neutrino tau, in *Proceedings, 26th International Cosmic Ray Conference (ICRC), August 17-25, 1999, Salt Lake City: Invited, Rapporteur, and Highlight Papers* (1999) p. 396, [2,396(1999)], arXiv:astro-ph/9906450 [astro-ph].

- [6] J. L. Feng, P. Fisher, F. Wilczek, and T. M. Yu, Observability of Earth Skimming Ultrahigh Energy Neutrinos, *Phys. Rev. Lett.* **88**, 161102 (2002), arXiv:hep-ph/0105067 [hep-ph].
- [7] C. Spiering, Towards High-Energy Neutrino Astronomy. A Historical Review, *Eur. Phys. J. H* **37**, 515 (2012), arXiv:1207.4952 [astro-ph.IM].
- [8] Y. Asaoka and M. Sasaki, Cherenkov τ shower earth-skimming method for PeV–EeV ν_τ observation with Ashra, *Astroparticle Physics* **41**, 7 (2013).
- [9] S. Ogawa, Observation of Optical Transients and Search for PeV-EeV Tau Neutrinos with Ashra-1, in *36th International Cosmic Ray Conference (ICRC2019)*, International Cosmic Ray Conference, Vol. 36 (2019) p. 970.
- [10] M. L. Ahnen *et al.* (MAGIC), Limits on the flux of tau neutrinos from 1 PeV to 3 EeV with the MAGIC telescopes, *Astropart. Phys.* **102**, 77 (2018), arXiv:1805.02750 [astro-ph.IM].
- [11] M. Mallamaci, D. Gora, and E. Bernardini (MAGIC), MAGIC as a high-energy ν_τ detector: performance study to follow-up IceCube transient events, in *MAGIC Contributions to the 36th International Cosmic Ray Conference (ICRC2019)* (2019) arXiv:1909.01314 [astro-ph.HE].
- [12] A. Aab *et al.* (Pierre Auger), Probing the origin of ultra-high-energy cosmic rays with neutrinos in the EeV energy range using the Pierre Auger Observatory, *JCAP* **1910** (10), 022, arXiv:1906.07422 [astro-ph.HE].
- [13] M. Schimp, Follow-up searches for ultra-high energy neutrinos from transient astrophysical sources with the Pierre Auger Observatory, in *36th International Cosmic Ray Conference (ICRC2019)*, International Cosmic Ray Conference, Vol. 36 (2019) p. 415.
- [14] Crouch, M.F. and Landecker, P.B. and Lathrop, J.F. and Reines, F. and Sandie, W.G. and Sobel, H.W. and Coxell, H. and Sellschop, J.P.F., Cosmic Ray Muon Fluxes Deep Underground: Intensity Versus Depth, and the Neutrino Induced Component, *Phys. Rev. D* **18**, 2239 (1978).
- [15] D. DeMuth *et al.*, Horizontal muons and a search for AGN neutrinos in Soudan 2, *Astroparticle Physics* **20**, 533–547 (2004).
- [16] M. Ambrosio *et al.*, Search for diffuse neutrino flux from astrophysical sources with MACRO, *Astroparticle Physics* **19**, 1 (2003).
- [17] W. Rhode, K. Daum, P. Bareyre, R. Barloutaud, G. Chardin, B. Degrange, J. Ernwein, B. Kuznik, H. Meyer, L. Mosca, L. Moscoso, O. Perdereau, M. Schubnell, S. Tisserant, and Y. Wei, Limits on the flux of very high energy neutrinos with the Fréjus detector, *Astroparticle*

- Physics **4**, 217 (1996).
- [18] M. R. Krishnaswamy, M. G. K. Menon, V. S. Narasimham, K. Hinotani, N. Ito, S. Miyake, J. L. Osborne, A. J. Parsons, and A. W. Wolfendale, The Kolar Gold Fields Neutrino Experiment. I. The Interactions of Cosmic Ray Neutrinos, Proceedings of the Royal Society of London. Series A, Mathematical and Physical Sciences **323**, 489 (1971).
- [19] C. Alberini *et al.* (LVD), The large-volume detector (LVD) of the Gran Sasso Laboratory, II Nuovo Cim. C **9**, 237 (1986).
- [20] H. León Vargas (HAWC), Prospects of Earth-skimming neutrino detection with HAWC, in *36th International Cosmic Ray Conference (ICRC 2019) Madison, Wisconsin, USA, July 24-August 1, 2019* (2019) arXiv:1908.07622 [physics.ins-det].
- [21] H. León Vargas (HAWC), Modeling the background for a neutrino search with the HAWC observatory, in *XIX International Workshop on Neutrino Telescopes Online, February 18-26, 2021* (2021).
- [22] A. U. Abeysekara *et al.*, Observation of the Crab Nebula with the HAWC Gamma-Ray Observatory, *Astrophys. J.* **843**, 39 (2017), arXiv:1701.01778 [astro-ph.HE].
- [23] H. A. Ayala Solares, H. Zhou, C. M. Hui, and P. Hüntemeyer (HAWC), Timing Calibration of the HAWC Observatory, in *33rd International Cosmic Ray Conference*, International Cosmic Ray Conference, Vol. 33 (2013) p. 2996.
- [24] A. U. Abeysekara *et al.* (HAWC), Data Acquisition Architecture and Online Processing System for the HAWC gamma-ray observatory, *Nucl. Instrum. Meth.* **A888**, 138 (2018), arXiv:1709.03751 [astro-ph.IM].
- [25] Instituto Nacional de Estadística, Geografía e Informática, Continuo de Elevaciones Mexicano 3.0 (CEM 3.0) (Accessed April 8, 2021), <https://www.inegi.org.mx/app/geo2/elevacionesmex/>.
- [26] H. León Vargas, A. Sandoval, E. Belmont, and R. Alfaro, Capability of the HAWC Gamma-Ray Observatory for the Indirect Detection of Ultrahigh-Energy Neutrinos, *Adv. Astron.* **2017**, 1932413 (2017), arXiv:1610.04820 [astro-ph.IM].
- [27] S. Agostinelli *et al.* (GEANT4), GEANT4: A Simulation toolkit, *Nucl. Instrum. Meth.* **A506**, 250 (2003).
- [28] R. Bütiköfer, Cosmic ray particle transport in the earth's magnetosphere, in *Solar Particle Radiation Storms Forecasting and Analysis: The HESPERIA HORIZON 2020 Project and*

- Beyond*, edited by O. E. Malandraki and N. B. Crosby (Springer International Publishing, Cham, 2018) pp. 79–94.
- [29] M. Aglietta *et al.*, Neutrino-induced and atmospheric single-muon fluxes measured over five decades of intensity by LVD at Gran Sasso Laboratory, *Astroparticle Physics* **3**, 311 (1995).
- [30] J. Elbert, M. Iacovacci, and V. Silvestrini, The Muon background from back scattered cosmic ray muons in a surface neutrino detector, *Europhys. Lett.* **14**, 181 (1991).
- [31] Peter K.F. Grieder, Chapter 3 - Cosmic Rays at Sea Level, in *Cosmic Rays at Earth*, edited by Peter K.F. Grieder (Elsevier, Amsterdam, 2001) pp. 305 – 457.
- [32] L. Bonechi, R. D’Alessandro, and A. Giammanco, Atmospheric muons as an imaging tool, *Reviews in Physics* **5**, 100038 (2020).
- [33] G. Carrasco Nuñez, personal communication (2020).
- [34] A. Lechmann, D. Mair, A. Ariga, T. Ariga, A. Ereditato, R. Nishiyama, C. Pistillo, P. Scampoli, F. Schlunegger, and M. Vladymyrov, The effect of rock composition on muon tomography measurements, *Solid Earth* **9**, 1517 (2018).
- [35] K. Morishima *et al.*, Discovery of a big void in Khufu’s Pyramid by observation of cosmic-ray muons, *Nature* **552**, 386 (2017).
- [36] Cosmic Ray Division (Yerevan Physics Institute), *Fluxes measured at Aragats, Muons* (Accessed April 8, 2021), <http://crd.yerphi.am/Muons>.
- [37] P. Lipari, Lepton spectra in the earth’s atmosphere, *Astroparticle Physics* **1**, 195 (1993).
- [38] P. Zyla *et al.* (Particle Data Group), Review of Particle Physics, *PTEP* **2020**, 083C01 (2020).
- [39] L. Rädcl and C. Wiebusch, Calculation of the Cherenkov light yield from low energetic secondary particles accompanying high-energy muons in ice and water with Geant4 simulations, *Astroparticle Physics* **38**, 53 (2012).
- [40] A. J. Smith, HAWC: Design, Operation, Reconstruction and Analysis (2015), arXiv:1508.05826 [astro-ph.IM].
- [41] M. G. Aartsen *et al.* (IceCube Collaboration), Characterization of the atmospheric muon flux in IceCube, *Astroparticle Physics* **78**, 1 (2016).